Computational Wavefront Shaping with Epi-mode 3D Refractive Index Microscopy

Mingxuan Cai,[1,*] Kevin C. Zhou,[1] Yi Xue,[2] and Laura Waller[1]

[1] *Department of Electrical Engineering and Computer Science, University of California, Berkeley, USA*
[2] *Department of Biomedical Engineering, University of California, Davis, USA*

[*] *mingxuan_cai@berkeley.edu*

Abstract: We present a wavefront shaping method that computes the optimal wavefront for random-access focusing through scattering in 3D, by using prior knowledge of the reconstructed 3D refractive index (RI), measured in epi-mode.

1. Introduction

The inhomogeneous refractive index distribution inside cells and tissues causes light to scatter, hindering optical focusing and imaging. By wavefront shaping with a spatial light modulator (SLM), light can be controlled to correct random wavefront distortions [1]. However, current approaches such as feedback-based wavefront shaping are too slow for imaging in vivo; optical phase conjugation using different types of guide stars generally corrects the distortion only within the memory effect range [2]. Therefore, it is valuable to explore a possible solution to achieve tight focusing at arbitrary locations inside a 3D scattering medium, based on pre-measuring the sample's 3D RI distribution and using it as prior knowledge for optimal wavefront generation.

Wavefront shaping is frequently used in fluorescence microscopy, but acquiring 3D refractive index information with epi-mode is challenging [3], hindering in vivo application. Recently, Xue *et al.* [4] proposed methods to recover the 3D refractive index from fluorescent images with epi-mode measurements. They consider fluorescent beads embedded in the sample as inner sources, emitting fluorescence that passes through the scattering medium. The 3D RI information is encoded from different angles via the spherical waves generated by the different fluorophores. With a physics-informed optimization framework, the 3D RI and fluorescence information are jointly reconstructed in an epi-mode implementation. Since the 3D RI represents the scattering potential of the sample, we can thus use it to compute the global optimal wavefront in order to form a tight focus at any given point in the volume. Here, we use simulations to demonstrate this wavefront shaping capability with epi-mode 3D RI measurements and propose an experimental realization.

2. Methods

Given a sample with spatially-varying RI, we assume a sparse distribution of N fluorophores at random 3D positions $(\vec{r},z)$, where each single fluorophore is activated sequentially (e.g. by point scanning). The fluorophore emits a spherical wave and acts as an inner source illuminating the sample. The field scatters through the sample and is imaged by an objective (Fig. 1(a)), generating the raw intensity measurements $\hat{I}_i(\vec{r},z)$ from which 3D phase information can be retrieved. Here, we compute the exit field $E_i(\vec{r},z)$ using the multi-slice scattering model [5], where a volume is approximated as a series of equally-spaced thin layers with a complex-valued RI $n_k(\vec{r})$ at the k-th layer. We define the i-th intensity forward prediction as $I_i(\vec{r},z) = |E_i(\vec{r},z)|^2$. To solve for the 3D RI of the sample, we formulate an optimization problem by minimizing the difference between raw measurements $\hat{I}_i(\vec{r},z)$ and forward predictions $I_i(\vec{r},z)$ with total variation regularization $TV(\cdot)$ with coefficient τ:

$$\hat{n}(\vec{r},z) = argmin_{n(\vec{r},z)} \sum_{i=1}^{N} ||\hat{I}_i(\vec{r},z) - \sum_{\lambda} I_{i,\lambda}(\vec{r},z,\lambda)||^2 + \tau TV(n(\vec{r},z)). \quad (1)$$

Considering the incoherent nature of fluorophores, we model their finite bandwidth by sampling the fluorophore's emission spectrum, generating the forward prediction at each sampled wavelength, and then obtaining the final image with a weighted sum of individual predictions added incoherently.

After reconstructing the 3D RI, we use a model-based phase conjugation method [6] to obtain the optimal wavefront to form a tight focus at any desired location inside the sample. We first generate a spherical wave virtually emitting from a target point location and use the multi-slice scattering model to compute the exit field based on the reconstructed 3D RI. Then, we refocus the output field to the focal plane E_f. Since the SLM is conjugate to the pupil plane of the objective, we then use a 2D Fourier transform to compute the corresponding

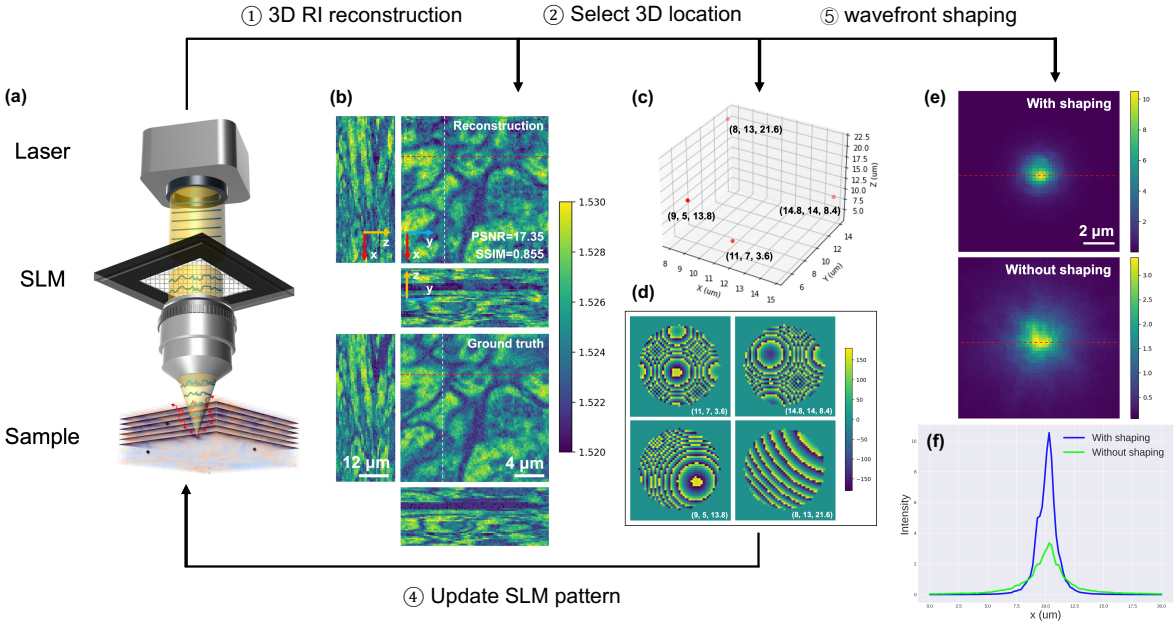

Fig. 1. (a) Proposed setup for computational wavefront shaping with epi-mode refractive index microscopy. (b) The reconstructed 3D refractive index and its ground truth. (c) Visualization of 4 arbitrarily selected 3D locations. (d) The phases of the computed wavefront that should be displayed on the SLM for each selected location. (e) Focus spot with and without wavefront shaping and their intensity cross-sections (f).

field $E_p = F_{2D}\{E_f\}$ at the pupil plane. After mapping the coordinates from E_p to E_{SLM}, we display the phase of E_{SLM} on the SLM, enabling incident light to form a diffraction-limited focus spot at the desired location.

3. Results

Our simulation results use realistic biological data, based on 3D isotropic TEM images of the CA1 region of Hippocampus [7]. To convert the TEM images to our ground-truth 3D RI map, we normalized the measurement to a spatially varying refractive index distribution from 1.520 to 1.529. The sample is surrounded by a medium of $n_b = 1.52$, with a volume of $100 \times 100 \times 40$ voxels with 0.2 μm (lateral) and 0.6 μm (axial) resolution. We randomly distribute $N = 50$ fluorescent beads inside the sample, which have an emission spectrum centered at 521 nm with a 48 nm bandwidth, and simulated imaging with an $NA = 0.6$ objective.

We initialize the reconstruction volume with the background RI $n_b = 1.52$. As shown in Fig. 1(b), the reconstruction recovers most of the details and fine structures of the ground truth. To compute the optimal wavefront for correction, we pick 4 points at arbitrary 3D locations inside the sample (see Fig. 1(c)). The result in Fig. 1(d) are the corresponding phase patterns that should be displayed on the SLM for wavefront correction. Figure 1(e,f) shows the expected improvement in the ability to form a tight focus at one of the target points.

References

1. H. Cao, A. P. Mosk, and S. Rotter, "Shaping the propagation of light in complex media," Nat. Phys. 18, 994–1007 (2022).
2. R. Horstmeyer, H. Ruan, and C. Yang, "Guidestar-assisted wavefront-shaping methods for focusing light into biological tissue," Nat. Photonics 9, 563–571 (2015).
3. P. Ledwig and F. E. Robles, "Partially coherent broadband 3D optical transfer functions with arbitrary temporal and angular power spectra," APL Photonics 8, 041301 (2023).
4. Y. Xue, D. Ren, and L. Waller, "Three-dimensional bi-functional refractive index and fluorescence microscopy (BRIEF)," Biomed. Opt. Express 13, 5900-5908 (2022).
5. S. Chowdhury, M. Chen, R. Eckert, D. Ren, F. Wu, N. Repina, and L. Waller, "High-resolution 3D refractive index microscopy of multiple-scattering samples from intensity images," Optica 6, 1211-1219 (2019).
6. A. Thendiyammal, G. Osnabrugge, T. Knop, and I. Vellekoop, "Model-based wavefront shaping microscopy," Opt. Lett. 45, 5101-5104 (2020).
7. A. Lucchi, K. Smith, R. Achanta, G. Knott, and P. Fua, "Supervoxel-Based Segmentation of Mitochondria in EM Image Stacks With Learned Shape Features," IEEE Trans. Med. Imaging 31, 474–486 (2012).